An Efficient Procedure To Measure Bubble Point Pressures for Hydrocarbon + CO_2 Mixtures

María A. Barrufet* and Januar F. S. Wirawan†

Petroleum Engineering Department, Texas A&M University, College Station, Texas 77843

Gustavo A. Iglesias-Silva

Departamento de Ingeniería Química, Instituto Tecnológico de Celaya, Celaya, Gto CP 38010, Mexico

Bubble point pressures for pentane + carbon dioxide, octane + carbon dioxide, and pentane + octane + carbon dioxide have been measured in the range 339–450 K. The apparatus has been designed to cover a wide range of temperatures and pressures with a single hydrocarbon load. Carbon dioxide and hydrocarbon compositions are determined gravimetrically by charging known masses into the equilibrium cell. Bubble points are reported for a total of 17 mixtures. To check the experimental technique, the vapor pressure of pentane was measured. Results agreed with the results reported by the Thermodynamics Research Center (*Data bases for Chemistry and Engineering TRC Thermodynamic Tables*, Version 1.3M; Thermodynamics Research Center: College Station, TX, Dec 1994) within 5%. This may not be considered good enough, but the sample purity was only 99+%. It is well-known that volatile impurities strongly affect bubble point pressures. Simple calculations with the Soave–Redlich–Kwong equation of state (SRK EOS) indicate that a 0.1% nitrogen impurity in pentane at 350 K would raise its vapor pressure (if evaluated as a bubble point) by 17%, while just 0.01% helium would raise this pressure by 6%. The experimental accuracies have been estimated to be approximately 1% in pressure and ±0.5 °C in temperature. These are considered sufficient for most engineering applications, particularly when working with crude oil mixtures.

Introduction

Reservoir engineers require fluid properties as a function of pressure and temperature to evaluate the production performance and the effective management of a reservoir. Of particular importance is the phase behavior of the fluids at reservoir conditions and at different pressures and temperatures that may be encountered during production, separation, and transmission.

Most reservoirs are abandoned after about 30% of the oil in place has been recovered. Current technical and economical constraints prevent the full development of a reservoir. Therefore, enhanced-oil-recovery (EOR) techniques need to be developed to improve the recovery of those reservoirs.

Several EOR techniques are available. These techniques include thermal processes like steam flooding and in-situ combustion, and miscible processes such as CO_2 flooding and natural gas flooding. In gas flooding, gas is injected into a well to mobilize the reservoir oil to a production well. When this gas is forced into the reservoir, a miscible front is generated by a gradual transfer of lighter hydrocarbon molecules from the oil to the gas. Under favorable pressures and temperatures, this front will be miscible with the oil, making it easier to move toward production wells.

CO_2 flooding changes the reservoir fluid properties in a complex manner. The mechanism of EOR is a multicontact miscibility displacement *(2)*. The miscible CO_2 process is related to the phase equilibria since the process involves intimate contact of gases and liquids *(3, 4)*. Most studies on the phase behavior of CO_2 with hydrocarbons have been limited to mixtures of CO_2 with pure hydrocarbons. These studies were usually made to obtain binary interaction parameters *(2, 5–11)*. Other studies have been made with crude oils. The results of these studies are very specific and can only be applied to the crude oils used *(11–16)*.

In this work, we have measured the bubble point pressures of binary mixtures of pentane + CO_2 and octane + CO_2, and ternary mixtures of pentane + octane + CO_2. The technique is also suitable for measurement of crude oils in which the oil mixture can be characterized by pseudocomponents.

Experimental Setup

The apparatus consists of four main parts: the vacuum system, the hydraulic system, a cell, and a gas boosting device.

The vacuum system consists of an 8800-series Welch DirecTorr II pump and two traps to protect the vacuum pump from liquids. The hydraulic system consists of a Ruska positive displacement pump no. 2236, a pressure gauge, and high-pressure valves. The purpose of this system is to change the volume in the upper portion of the recombination cell by displacing the floating piston inside the recombination cell with hydraulic oil. The volume of this cell is 1000 cm^3. Pressure changes in the recombination cell are accomplished by these volumetric changes. The pump has a capacity of 1000 cm^3, and the maximum working pressure is 83 MPa. The pump is equipped with a volume scale to monitor the volume of the discharge and, indirectly, the volume of the cell. This scale can be read within ±0.01 cm^3.

The gas sample (CO_2) is delivered from a large gas tank to a 300 cm^3 sample cylinder that can be weighed on a Mettler scale PM4600 (4 kg maximum ±0.1 g accuracy). The pressure is boosted inside this cylinder to provide enough overpressure to charge the sampling cell. The gas booster is an air-operated gas compressor which works on a differential area piston principle.

* To whom correspondence should be addressed.
† Present address: Total Indonesie, Jakarta 10010, Indonesie.

0021-9568/95/1740-1072$09.00/0

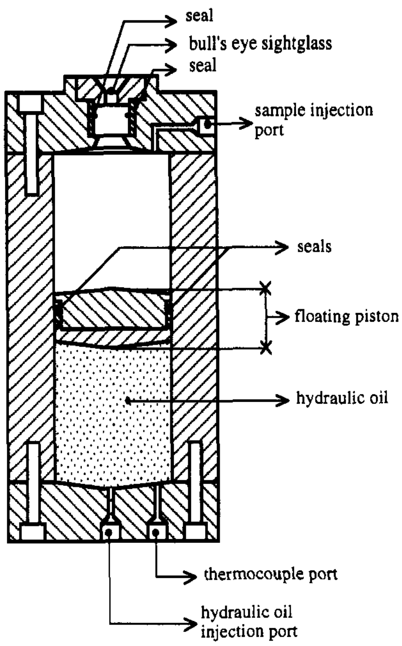

Figure 1. Schematics of the recombination cell.

The recombination apparatus used in this experiment is a JEFRI recombination apparatus that consists of three main parts: a temperature-controlled air-bath oven, a cell, and a rocking mechanism.

The temperature-controlled air-bath oven has a maximum operating temperature of 200 °C. The temperature is uniformly distributed throughout the oven within ±0.5 °C. The temperature can be set to the desired temperature using a microprocessor temperature controller. For experiments at subambient conditions, a recirculation cooling fluid can be circulated through built-in coils from a refrigerant unit.

Figure 1 shows the details of the recombination cell. It has an isolating floating piston which can be moved up and down the cell when hydraulic oil is injected through the hydraulic oil port at the bottom of the cell. The sample is charged into the upper portion of the cell, and the pressure of the sample can be changed by displacing the piston. A Heise digital pressure gauge is part of the JEFRI apparatus. The cell has a maximum working pressure of 69 MPa and a maximum temperature of 200 °C. It is equipped with a sight glass eye centered in the top end cap of the cell and a sight glass viewing mirror to enable the operator to visualize bubbles formed when two phases exist. Temperature is determined with a thermocouple which is in direct contact with the fluid.

The rocking mechanism agitates the contents of the recombination cell by oscillating the cell a full 60° about its center of gravity at a rate of about 40 cycles/min. This provides efficient mixing to obtain rapid equilibrium.

Experimental Technique

Pentane and octane (packaged under nitrogen) from Aldrich Chemical Co. had a minimum purity of 99%. The water content was less than 0.005%, and the evaporation residue less than 0.0003%. The CO_2 used was certified O_2 free with a minimum purity of 99.99%.

The liquid components of the sample were charged into the cell before the gas to avoid the possibility of backflush. The amounts of liquid and gas charged into the recombination cell were measured gravimetrically by weighing the containers before and after charging. The balance used for the liquid was a Mettler PM4600 and could measure to ±0.01 g. For the gas, since the gas cylinder is heavier, a Mettler scale with an accuracy of ±0.1 g was used .

Table 1. Rounded and Exact Mole Fractions for the Pentane (1) + Octane (2) + Carbon Dioxide (3) Mixtures Used

exact mixture composition			rounded mixture composition		
x_1	x_2	x_3	x_1	x_2	x_3
0.000	1.000	0.000	0.00	1.00	0.00
0.000	0.557	0.443	0.00	0.56	0.44
0.000	0.371	0.629	0.00	0.37	0.63
0.000	0.176	0.824	0.00	0.18	0.82
0.252	0.748	0.000	0.25	0.75	0.00
0.500	0.500	0.000	0.50	0.50	0.00
0.364	0.363	0.273	0.36	0.37	0.27
0.227	0.227	0.546	0.22	0.23	0.55
0.121	0.120	0.759	0.12	0.12	0.76
0.746	0.254	0.000	0.75	0.25	0.00
0.555	0.189	0.256	0.55	0.19	0.26
0.419	0.143	0.438	0.42	0.14	0.44
0.269	0.092	0.639	0.27	0.09	0.64
0.161	0.055	0.784	0.16	0.06	0.78
1.000	0.000	0.000	1.00	0.00	0.00

The objective was to measure the largest possible number of bubble point pressures using a single hydrocarbon load with different amounts of CO_2. This required a knowledge of the minimum and maximum mass loadings that would allow observation of these bubble points given the constraint of the size of the recombination cell. The calculation of the sample size was based on simulated pressure–temperature bubble points for the mixtures. A commercial simulator *(17)* was used to estimate the bubble points of the desired mixtures using the Peng–Robinson equation of state (EOS), and the upper and lower bounds in the pressure and temperature depended upon the working capacities of the equipment.

Volumes of 100 and 600 cm^3 were used as conservative estimates for the highest and lowest piston positions, respectively. The liquid molar volumes of each mixture at the selected bubble points were estimated using the Peng–Robinson EOS, and these volumes were used to estimate the mass to be charged into the cell.

The maximum and minimum masses of the hydrocarbon in the mixture were estimated as follows:

$$m_i = (1 - x_{CO_2})x_{HC_i}\left(\frac{V_{cell}}{V_m}\right)M_i \tag{1}$$

where V_{cell} is the cell volume (100 or 600 cm^3), V_m is the molar volume of the mixture, x_{CO_2} is the mole fraction of CO_2 in the mixture, and x_{HC_i} is the mole fraction of component i of molecular weight M_i in the hydrocarbon mixture excluding the CO_2. For each bubble point pressure and temperature a minimum mass and a maximum mass were calculated. These values were calculated for each hydrocarbon mixture with different amounts of CO_2. The critical value of the minimum mass is the largest number corresponding to the small volume, and vice versa, the critical value of the maximum mass is the smallest number associated with the large volume. Since one mixture of hydrocarbon was used with several CO_2 concentrations, the initial hydrocarbon load has to be within these upper and lower bounds.

The mass of CO_2 was determined gravimetrically, but this was first estimated using the injection pressure and the volume of pure CO_2 determined from the Soave–Redlich–Kwong (SRK) EOS. First, the densities of pentane and octane at ambient conditions were determined using a pycnometer at 20 °C. This density along with the mass charged was used to estimate the volume occupied by pentane and octane in the cell. We assumed that both pentane and octane were in the liquid state during CO_2 injection and that the change in liquid volume caused by

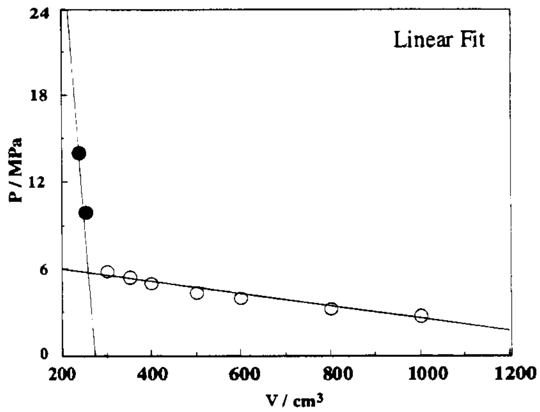

Figure 2. Bubble point pressure at 348 K for pentane (1) + octane (2) + carbon dioxide (3), with x_1 = 0.42 and x_2 = 0.14: (●) $P = 113.205 - 0.413V$ (R^2 = 1.0), (○) $P = 6.8486 - 0.004296V$ (R^2 = 0.961).

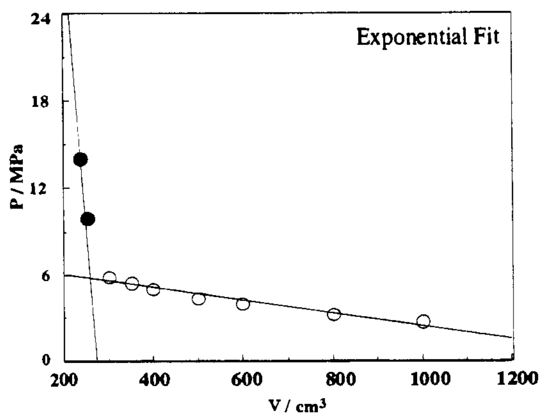

Figure 3. Bubble point pressure at 348 K for pentane (1) + octane (2) + carbon dioxide (3), with x_1 = 0.42 and x_2 = 0.14: (●) $P = 113.205 - 0.413V$ (R^2 = 1.0), (○) $P = 7.758 \times 10^{(-4.5523\times-4V)}$ (R^2 = 0.991).

the solubility of CO_2 was negligible. With these assumptions, the volume to be occupied by CO_2 gas was calculated by subtracting the volumes of pentane and octane from 600 cm^3, which was the largest allowed volume in the cell.

Results

Table 1 lists the mixture compositions and their rounded values for simplicity. The measured variables are the volume and the pressure at a constant temperature. The bubble point pressure and volume were obtained by curve fitting the pressure–volume data in the liquid and in the two-phase regions. The intersection of the curves represents the bubble point pressure. Figures 2 and 3 show an example at 348 K. The liquid phase was always fitted with a straight line, but the two-phase region was fitted with either an exponential or a straight line. The intersection of the liquid phase line with the exponential curve provides different bubble point pressures from the intersection with the straight line, but these pressures generally agree within 1%. Both pressures provide an estimate of experimental uncertainty.

Table 2 presents the experimental bubble point pressures obtained for the 17 mixtures using a linear fit and an exponential fit for the two-phase pressure–volume line. The difference between these bubble point pressures is generally within 1%.

Figure 4 shows the effect of hydrocarbon composition on the bubble point line. The higher the light component mole fraction in the mixture, the higher is the bubble point pressure for a particular temperature. In addition, the slopes of the curves increase with the increase in the amount of the light component. The effect of carbon dioxide content on a 50 mol % pentane + 50 mol % octane hydrocarbon mixture is shown in Figure 5. The pressure increases with the increase in carbon dioxide content.

A comparison between the results obtained in this study and published results for pure pentane is shown in Figure 6. The base line corresponds to the data reported by the Thermodynamics Research Center *(1)*. The results of this work agree with TRC data within approximately 5% with the exception of the vapor pressure measured at 373.15 K. By extrapolation, these results are also within 5% agreement with those of Leu and Robinson *(5)* and Cheng *et al.*

Table 2. Comparison of Measured Bubble Point Pressures (*P*) for Pentane (1) + Octane (2) + Carbon Dioxide (3) Mixtures

				P/MPa	
x_1	x_2	x_3	*T*/K	linear fit	exponential fit
0.000	1.000	0.000	423.15	0.2	0.2
			448.15	0.4	0.4
0.000	0.560	0.440	348.15	6.1	6.3
			373.15	7.4	7.6
			398.15	8.3	8.6
			423.15	8.9	9.3
			448.15	9.4	9.7
0.000	0.370	0.630	348.15	9.4	9.7
			373.15	11.3	11.5
			398.15	12.4	12.8
			423.15	13.5	13.8
			448.15	13.4	14.1
0.000	0.180	0.820	348.15	12.3	12.5
			373.15	14.9	15.0
			398.15	16.4	16.6
0.250	0.750	0.000	398.15	0.3	0.3
			423.15	0.5	0.5
			448.15	0.8	0.8
0.500	0.500	0.000	373.15	0.3	0.3
			398.15	0.6	0.6
			423.15	0.9	0.9
			448.15	1.3	1.3
0.365	0.365	0.270	348.15	3.6	3.7
			373.15	4.3	4.5
			398.15	4.9	5.2
			423.15	5.6	5.8
			448.15	5.9	6.2
0.225	0.225	0.550	348.15	7.6	7.7
			373.15	8.9	9.2
0.225	0.225	0.550	398.15	10.1	10.5
			423.15	10.8	11.1
			448.15	10.7	11.3
0.120	0.120	0.76	348.15	10.2	10.3
			373.15	12.5	12.6
			398.15	14.1	14.3
0.750	0.250	0.000	373.15	0.5	0.5
			398.15	0.8	0.9
			423.15	1.3	1.3
			448.15	1.8	1.9
0.555	0.185	0.260	348.15	3.4	3.5
			373.15	4.0	4.2
			398.15	4.8	5.0
			423.15	5.5	5.7
			448.15	6.1	6.3
0.420	0.140	0.440	348.15	5.7	5.9
			373.15	7.0	7.2
			398.15	8.0	8.2
			423.15	8.7	9.0
			448.15	8.9	9.2
0.270	0.090	0.640	348.15	8.4	8.5
			373.15	10.0	10.2
			398.15	11.5	11.8
			423.15	11.4	11.8
0.165	0.055	0.780	348.15	10.2	10.3
1.000	0.000	0.000	348.15	0.3	0.3
			373.15	0.7	0.7
			398.15	1.1	1.1
			423.15	1.7	1.7
			448.15	2.5	2.5

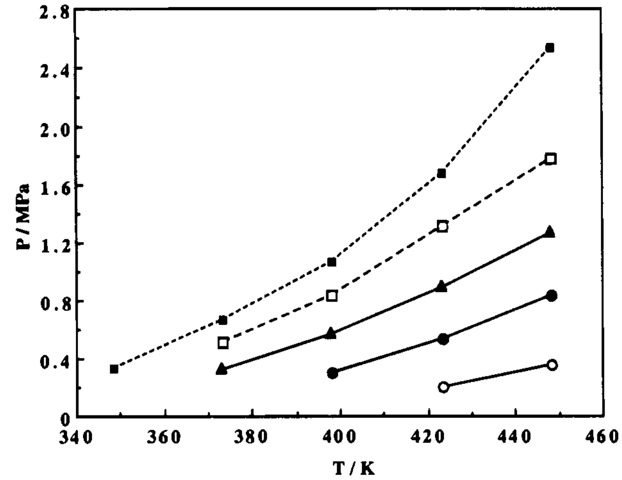

Figure 4. Effect of hydrocarbon composition on the bubble point pressure for pentane (1) + octane (2): (○) $x_1 = 0.0$, (●) $x_1 = 0.25$, (▲) $x_1 = 0.5$, (□) $x_1 = 0.75$, (square with plus sign inside) $x_1 = 1$.

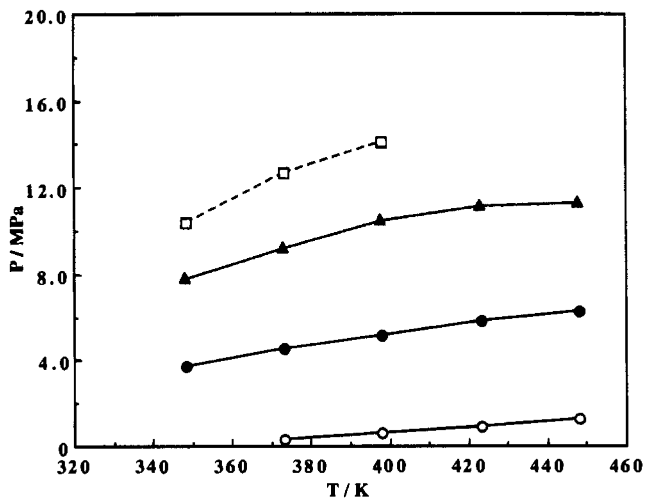

Figure 5. Effect of carbon dioxide content on bubble point pressures for pentane (1) + octane (2) + carbon dioxide (3): (○) $x_1 = x_2$ 0.5, (●) $x_1 = x_2 = 0.365$, (▲) $x_1 = x_2 = 0.225$, (□) $x_1 = x_2 = 0.12$.

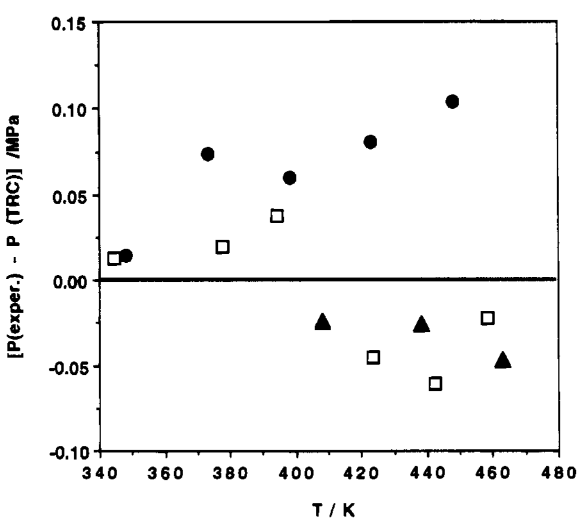

Figure 6. Comparison between this work and literature results for pentane: (●) this work, (□) ref 6, (▲) ref 5, (—) ref 1.

(6) . This may not look so encouraging; however, it is well-known that small amounts of volatile impurities cause a substantial increase in bubble points. Since the vapor pressures were measured as bubble points, this may have been the major source of discrepancy. A simple calculation

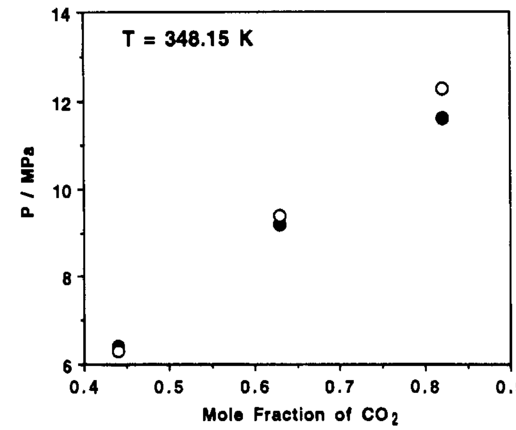

Figure 7. Comparison between this work and literature results for pentane + carbon dioxide: (○) this work, (●) ref 6.

using the SRK EOS provides a vapor pressure of pentane at 350 K of 0.3426 MPa, and a 0.1% impurity of N_2 gives a bubble point pressure of 0.399 MPa, nearly a 17% change. The estimated dew point pressure for this mixture is 0.3430 MPa, only 0.1% higher than the vapor pressure of pure pentane. Additionally, the measurements could be improved by using a more accurate pressure gauge. These saturation pressures are less than 2.5 MPa, and our apparatus is more accurate at higher pressures. Figure 7 shows a comparison of bubble point pressures measured in this work with those of Cheng *et al. (5)*; again the agreement is within 5%. Considering the limitations regarding the purity of the samples used and the accuracies in the weight, temperature, and pressure, this is considered sufficient for most engineering applications.

Acknowledgment

We thank Kai Liu for helping in the preparation of all figures and tables.

Literature Cited

(1) *Data bases for Chemistry and Engineering - TRC Thermodynamic Tables*, Version 1.3M; Thermodynamics Research Center: College Station, TX, Dec 1994.
(2) Chai, C. P.; Paulaitis, M. E. *J. Chem. Eng. Data* **1981**, *26*, 277.
(3) Metcalfe, R. S.; Yarborough, L. *Trans. AIME* **1979**, *267*, 242.
(4) Holm, L. W. Miscible Displacement. In *Petroleum Engineering Handbook*; Bradley, H. B., Ed.; Society of Petroleum Engineers: Richardson, TX, 1987; pp 45.1–45.15.
(5) Leu, A. D.; Robinson, D. B. *J. Chem. Eng. Data* **1987** *32*, 447.
(6) Cheng, H.; de Fernandez, M. E. P.; Zollweg, J. A.; Streett, W. B. *J. Chem. Eng. Data* **1989**, *34*, 319.
(7) Weng, W. L.; Lee, M. J. *J. Chem. Eng. Data* **1992**, *37*, 213.
(8) Kim, C. H.; Clark, A. B.; Vimalchand, P; Donohue, M. D. *J. Chem. Eng. Data* **1989**, *34*, 391.
(9) Monger, T. G. *Soc. Pet. Eng. J.* **1985**, 865.
(10) Hsu, J. J. C.; Nagarajan, N.; Robinson, R. L. Jr. *J. Chem. Eng. Data* **1985**, *30*, 485.
(11) Hottovy, J. D.; Luks, K. D.; Kohn, J. P. *J. Chem. Eng. Data* **1981**, *26*, 256.
(12) Silva, M. K.; Orr, F. M., Jr. *SPE Reservoir Eng.* **1987**, 468.
(13) Silva, M. K.; Orr, F. M., Jr. *SPE Reservoir Eng.* **1987**, 479.
(14) Benham, A. L.; Dowden, W. E.; Kunzman, W. *Trans. AIME* **1960**, *219*, 229.
(15) Omole, O.; Osoba, J. S. *J. Can. Pet. Technol.* **1989**, 97.
(16) Sebastian, H. M.; Wenger, R. S.; Renner, T. A. *JPT* **1985**, 2076.
(17) *PROSIM® - A General Purpose Hydrocarbon Process Simulator*; Bryan Research & Engineering, Inc.: Bryan, TX, Jan 1, 1991.

Received for review February 6, 1995. Accepted May 4, 1995.[⊗] Financial support from the Department of Energy (Grant DE-FG03-93AR14357) is acknowledged.

JE950037C

[⊗] Abstract published in *Advance ACS Abstracts*, July 1, 1995.